Molecular Dynamics Simulations of the Interior of Aqueous Reverse Micelles: A Comparison between Sodium and Potassium Counterions

James Faeder,[1] Mark V. Albert, and Branka M. Ladanyi[*]

Department of Chemistry, Colorado State University, Fort Collins, CO 80523

Abstract

We present the results of a molecular dynamics (MD) simulation study of the effects of counterion type on the properties of the interior region of aqueous reverse micelles. The model systems, which treat only the interior region at the atomistic level, are designed to represent water-in-oil microemulsions formed by the aerosol-OT (AOT) surfactant, either with its usual counterion, Na^+, or with the K^+ counterion. Our study covers the water content, w_0 = [H_2O]/[surfactant], range of 1 to 7.5, where the reverse micelles are approximately spherical and contain tens to hundreds of water molecules in their interior pool. We find that several key structural and dynamical features of the reverse micelle water pool are strongly affected by counterion type. These effects can be ascribed to the differences in head group-counterion coordination and to the stronger affinity for water that the smaller Na^+ ion exhibits. At low water content, K^+ ions are able to coordinate four head groups, while Na^+ coordinates a maximum of three. As w_0 increases, this coordination number decreases for both ions, but always remains higher for K^+, which also has a stronger tendency to remain in the interfacial region than does Na^+. K^+ displaces water from the interface to a larger extent than does Na^+, with the result that fewer water molecules are trapped in between the head groups. That and the fact that K^+ has a weaker attraction for water than does Na^+, lead to higher mobility of water throughout the reverse micelle interior and more bulk-like structural features, such as the number of water-water hydrogen bonds, in the interfacial region.

I. Introduction

Aqueous reverse micelles (RMs), which are nanoscopic water pools in a continuous nonpolar phase stabilized by a surrounding layer of surfactant molecules,[1-6] provide a simple model system in which to study how geometry and interfacial complexity affect the properties of

---

[1] Present address: Theoretical Division, Los Alamos National Laboratory, Los Alamos, NM 87545.
[*] To whom correspondence should be addressed. E-mail: bl@lamar.colostate.edu.

water near an interface. They also have numerous practical applications—e.g., heterogeneous chemical and biochemical catalysis, drug delivery, and nanocluster synthesis.[7-11]

In two recent molecular dynamics (MD) computer simulation studies we have examined the structural and dynamical properties of water and counterions in the RM interior as a function of micelle size.[12,13] These studies focused on model RMs that were designed to represent those formed by the aerosol OT (AOT) surfactant. AOT is an anionic surfactant, with Na^+ as its usual counterion, that forms approximately spherical RMs, whose radius in the presence of a given oil phase depends solely on the ratio [9,14]

$$w_0 = [H_2O]/[\text{surfactant}]. \qquad (1)$$

In agreement with a large body of experimental observations,[9] water in the model RMs formed well-defined layers in the vicinity of the surfactant sulfonate head groups, where water mobility was greatly reduced. Translational and rotational mobilities within a given layer also exhibited strong variations with micelle size. These variations were related to both the increase in the size of the core region, where water properties are closer to the bulk, and to the increase with w_0 of the surface area per head group,[14] which leads to higher mobility of the interfacial water.[12]

The effects of substituting other counterions for Na^+ in AOT-based reverse micelles are of considerable technological interest since such a substitution is a key step in common nanocluster synthesis methods.[11] Several experimental studies have explored how counterion substitution affects the properties of AOT surfactant assemblies.[15-25] For example, substitution by transition metal dications was shown by small-angle neutron scattering to change the structure of small RMs from spherical to cylindrical, an effect which was attributed to the reduced effectiveness of the strongly hydrated dications at screening head group repulsions.[16] RMs with alkali metal cations, on the other hand, remain spherical over the same range of water content.[16] Nonetheless, relatively few studies have examined how counterion size affects the structural properties of the RM interior. Infrared absorption studies of water/MAOT/isooctane RMs for a series of alkali cations M^+ found that counterion size had only a small effect on head group hydration as measured by changes in the OH stretch region of the water spectrum.[25] On the other hand, studies of solvation dynamics in water/MAOT/isooctane RMs found that water mobility decreased according the trend $NH_4^+ > K^+ > Na^+ > Ca^{2+}$.[23,24]

In this paper we investigate the effect of changing the counterion from sodium to potassium on the equilibrium properties of the RM interior using MD simulation. Increasing the radius of the counterion substantially affects the structure and properties of the interfacial region

since the interactions with the head group ions and water are weaker while at the same time the volume occupied by the counterions is larger. These two differences compete in their effect on water mobility since weaker ionic interactions will tend to increase water mobility, while the larger counterion size will tend to exclude more water from the interface, where our previous studies found that water was least mobile.

The remainder of the article is organized as follows: In Sec. II, we review the simulation model, present additional parameters specific to the K^+ counterions, and give details of the simulation runs used to determine the equilibrium properties. Section III contains the simulation results and a detailed comparison between the properties of Na^+ and K^+ RMs. Section IV concludes with a summary of our main findings and a comparison of these with experimental observations.

II. Simulations

We have modeled the interior of an aqueous reverse micelle as a rigid spherical cavity and treated only the surfactant head groups, counterions, and water at a molecular level. Details of the model and the procedures used to produce equilibrated reverse micelles have been presented elsewhere.[12] In our model the head groups protrude from the cavity boundary and are tethered only in the radial direction. These features allow the counterions to occupy bridging positions between the head groups and permit the spacing between head groups to be nonuniform. The radial positions of the head groups are restricted using a harmonic potential

$$u(d) = \tfrac{1}{2} k_e (d - d_e)^2,$$ (2)

where d is the distance from the cavity wall, $d_e = 2.5\,\text{Å}$ is the equilibrium distance, and $k_e = 600\ \text{kcal mol}^{-1}\ \text{Å}^{-2}$ is the force constant. The interaction potential between the cavity and the free molecules in the interior is determined by assuming the region outside the cavity is composed of a uniform continuum of nonpolar molecules that interact with interior molecules through a Lennard-Jones (LJ) 6-12 potential. The resulting potential[12] is the spherical analogue of the standard 3-9 potential that is commonly used for flat interfaces.[26] The molecular interactions inside the cavity are described in terms of potentials of the LJ + Coulomb form, with the interaction between sites of type α and β on different molecules or ions given by

$$u_{\alpha\beta}(r) = 4\left(\varepsilon_\alpha \varepsilon_\beta\right)^{1/2} \left[\left(\frac{\sigma_\alpha + \sigma_\beta}{2r}\right)^{12} - \left(\frac{\sigma_\alpha + \sigma_\beta}{2r}\right)^6 \right] + \frac{q_\alpha q_\beta}{4\pi\varepsilon_0 r},$$ (3)

3

where ε_α and σ_α are the LJ well depth and diameter and q_α the partial charge for site α. As indicated in the above equation, we are using the Lorentz-Berthelot combining rules to obtain the LJ parameters for unlike sites. The head groups, which we denote as Z$^-$, are represented as a single interaction site carrying a charge of $-e$, although work on removing this approximation by using a 4-site model for SO_3^- is currently under way.[27] We use the SPC/E model for water.[28] The potential parameters, summarized in Table 1, are identical to our previous simulation[12] with the addition of parameters for K$^+$. In going from Na$^+$ to K$^+$ the only change was to increase the LJ diameter by an amount determined from a previous parameterization of cation–SPC/E water potentials.[29]

Table 1. Potential Model Parameters

Interaction Site	σ (Å)	ε/k_B (K)	q (e)
O	3.166	78.24	-0.8476
H	—	0.00	0.4238
Z$^-$	6.000	251.58	-1.0000
Na$^+$	2.275	58.01	1.0000
K$^+$	3.023	58.01	1.0000
Wall^a	2.500	231.55	0.0000

^{a} Only O, Na, and K atoms interact with the wall, and the interaction is the same for all three atom types. The exact wall potential is given in Ref. [12].

Four different RM sizes were simulated with K$^+$ counterions, w_0=1, 2, 4, and 7.5, corresponding to the sizes used in our previous studies, where the numbers of surfactant (n_S) molecules corresponding to a given w_0 were interpolated from the estimates of Eicke and Rehak,[14] which were based on light scattering and sedimentation experiments. For this range of water content, which lies in the lower region of the phase diagram for water-in-oil microemulsions, the aggregates are approximately spherical, containing tens to hundreds of water molecules.[9] In order to make a controlled comparison, we have assumed that the number of surfactant molecules per aggregate does not change when K$^+$ replaces Na$^+$ as the counterion. As in the previous studies, the RM radii are determined by assigning w_0-independent molecular volumes to water (30 Å^3), K$^+$ (14.5 Å^3), and Z$^-$ (57 Å^3). The radius, R, is then given by

$$R = (3V/4\pi)^{1/3} + \sigma_{wall}, \tag{4}$$

where V is the total volume occupied by the molecular components. A list of the parameters for the K$^+$ RMs in the current study is given in Table 2. Parameters for the Na$^+$ RMs were the same as in our previous simulations.[12]

Table 2. Composition and Size of the K^{+} Reverse Micelles.

w_0	n_S	n_{water}	R (Å)
1.0	21	21	10.48
2.0	27^a	53^a	11.94
4.0	37^a	149^a	14.43
7.5	70^a	524^a	19.54

^{a} These numbers differ slightly from those of Ref. [12] due to slight differences in the way the interpolation from the experimental data was performed, but these differences have a negligible effect on any observable properties.

RMs were constructed using a three-step process:[12] (1) placement and optimization of head group ions, (2) placement of counterions followed by simulated annealing to find the lowest energy structure, (3) placement of water followed by equilibration at 500 K, cooling to 300 K, and equilibration at 300 K. The total process typically involved about 0.5 ns of MD simulation time to produce an equilibrated starting point for production runs, which were 5 ns in length for the two smaller sizes and 1 ns for the two larger sizes, with configurations saved at 100 fs intervals. Integration of the MD trajectories was performed using the velocity Verlet algorithm with a 2 fs step size and appropriate bond constraints.[30] The temperature was regulated using the Berendsen thermostat[31] with a time constant of 0.4 ps during the equilibration periods and 2 ps during the production runs.

We expect that the present model, despite its relative simplicity, represents a reasonable approach to the study of the changes in the structure and dynamics within the RM water pool brought about by a change in the counterion size. As noted earlier, unlike the singly charged counterions considered here, dications distort the AOT RM shape. To study the effects of counterion charge on the RM shape, we would need to modify our model to allow for shape distortion. Atomistic surfactant tail models, which have recently been used in studies of other types of RMs,[32-34] would be a possible approach to the study of dication effects on the AOT RM water pool properties.

III. Results and Discussion

Figure 1 shows snapshots of two w_0=2 reverse micelles with potassium and sodium counterions. In both cases the overwhelming majority of the counterions are located at the interface, where they interact strongly with the head group anions, while only a small percentage of counterions dissociate from the ionic outer layer to dissolve in the interior (see Table 3). The snapshots in Fig. 1 show that the counterions at the interface are highly coordinated and form a

lattice-like structure that greatly restricts the mobility of both water and counterions in this region. It is thus not surprising that the primary differences that arise from the change of counterions occur in the interfacial layer, but it is perhaps less anticipated that the K^+ counterions form the more highly coordinated lattice. This is simply a consequence of the fact that more anions can pack around the larger K^+ counterions. The most salient feature of the snapshots in Fig. 1 is the presence of three quadruply-coordinated K^+ counterions and the absence of such highly coordinated Na^+ counterions. In addition, the larger K^+ counterions occupy more surface area on the interface, permitting less water penetration. The combination of higher ionic coordination, less water at the interface, and weaker interaction with water, leads to less dissociation of K^+ into the RM core and less disruption of the water structure in the layer adjacent to the interface.
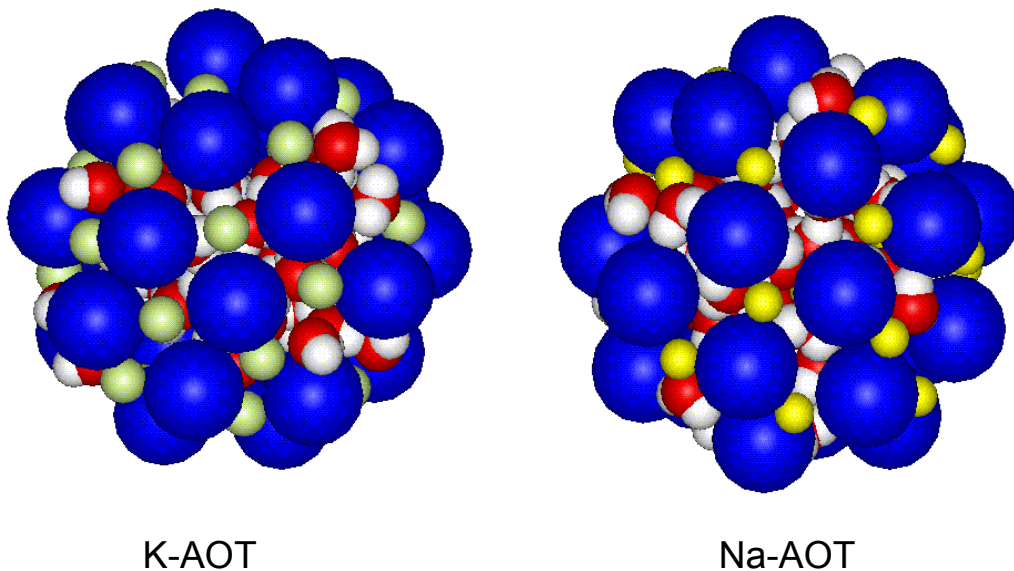

K-AOT   Na-AOT

Figure 1. Snapshots of the RM interior for $w_0 = 2$. Key: blue—head group anions, red—water oxygen, white—water hydrogen, light green—K^+, yellow—Na^+.

The overall greater ionic coordination in the K^+ RMs and the absence of quadruple coordination the Na^+ RMs are quantified for all the RM sizes studied by the coordination data presented in Table 3. The cutoff distance for coordination is taken to be the position of the minimum following the first peak in the counterion–head group (Z^-) pair distribution function, 4.8 Å for Na^+ and 5.5 Å for K^+. The table also shows that the fraction of dissolved counterions, i.e. counterions with zero head group coordination, is much smaller at all sizes studied for K^+

than Na^+, which may be a surprise given the weaker K^+–anion interaction, but is a result of the more favorable coordination at the interface described above.

Table 3. Fraction of counterions with given coordination numbers to head group anions for K^+ and Na^+ (in parenthesis) RMs.

Coordination number	w_0			
	1	2	4	7.5
0	0.02 (0.05)	0.00 (0.07)	0.00 (0.10)	0.03 (0.18)
1	0.01 (0.02)	0.00 (0.07)	0.02 (0.30)	0.09 (0.36)
2	0.01 (0.18)	0.01 (0.31)	0.21 (0.30)	0.26 (0.31)
3	0.61 (0.75)	0.71 (0.55)	0.71 (0.30)	0.57 (0.14)
4	0.35 (0.00)	0.28 (0.00)	0.06 (0.00)	0.04 (0.00)
Mean coordination	3.3 (2.6)	3.3 (2.3)	2.8 (1.8)	2.5 (1.4)

The radial density profiles shown in Fig. 2 reveal that the basic layered structure of water and counterions in the RM interior is not disrupted by the larger K^+ counterions, although some structural differences are observed. In this figure, the density of water oxygen atoms and counterions respectively are plotted as a function of the distance, D, from the equilibrium position of the head group anions on a sphere of radius 2.5 Å smaller than the enclosing cavity. In our previous study we identified three distinct water regions based on the water density profiles: a layer of *trapped* water with a density peak near $D = 0$ Å, a layer of *bound* water with a prominent peak at $D = 3$ Å that extended to the minimum following a secondary peak at around $D = 4$ Å, and a core region containing *free* water where the density profile exhibits small fluctuations about the bulk value. The water density profiles shown in the left panel of Fig. 2 also support this classification for the K^+ RMs. The larger K^+ counterions pack more efficiently in the interfacial region, excluding water from this region to a greater extent. This is reflected in the smaller trapped water peaks at all RM sizes. The differences in the amount of trapped water are quantified in Table 4. The position of the trapped water peak is also slightly shifted away from the interface in the K^+ RMs. There is a nearly complete exclusion of water from the volume separating the trapped and bound layers, and the magnitudes of the density peaks at $D = 3$ Å are almost identical, suggesting that these features result primarily from excluded volume interactions between water and the relatively large head group anions. The positions of the second peak and subsequent minimum in the bound water region are similar for the $w_0 = 1$ and 2 RMs, but different in the $w_0 = 4$ and 7.5 RMs, where in the K^+ RMs the second minimum extends out to nearly 6 Å. In addition to the packing effects mentioned above, water in this region is strongly affected by its interactions with ions. It appears that at small RM sizes packing considerations dominate the density profiles, while the comparatively weaker interaction of the

8

K$^+$ counterions with water becomes important only at the larger sizes. The counterion-water pair densities shown in Fig. 3 indicate that the regions of the first solvation shells around the Na$^+$ counterions are more highly structured than those around the K$^+$ counterions. For simplicity the boundaries of the bound water region used to classify water in Table 4 and in the calculation of mobilities are the same for both the Na$^+$ and K$^+$ reverse micelles.
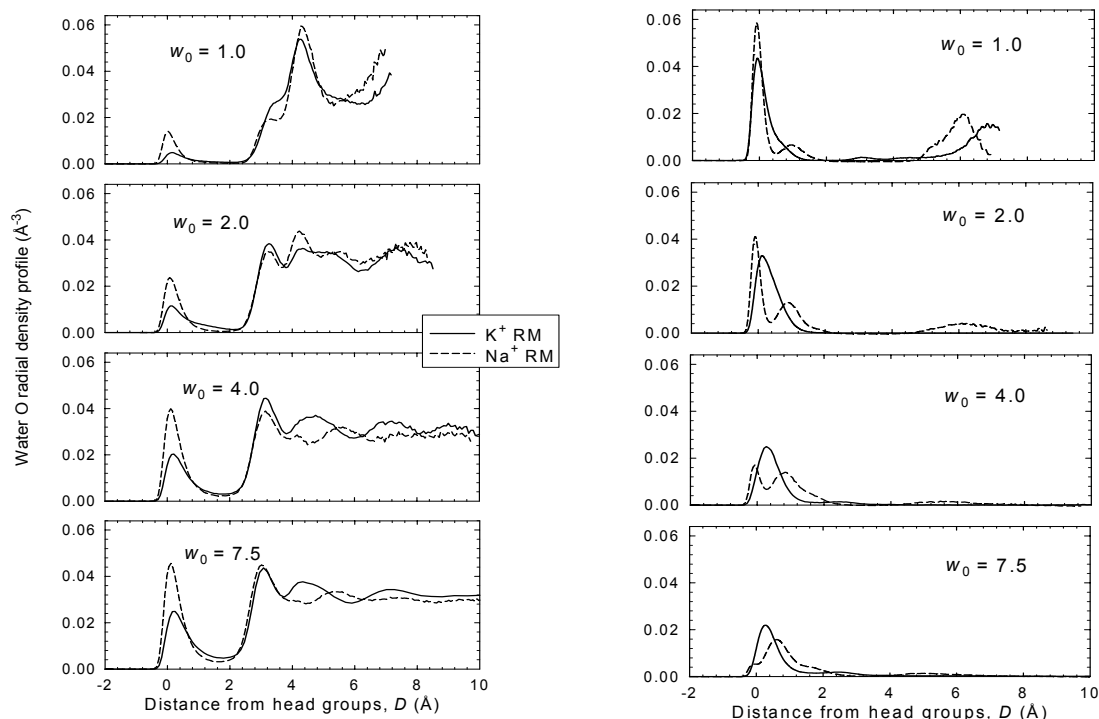

Figure 2. Density (in Å^{-3}) of water oxygens (left) and counterions (right) as a function of distance from the interface, D, measured in Å. Solid lines are for K$^+$ RMs, dashed lines are for Na$^+$ RMs. D is measured from the surface 2.5 Å inside the cavity boundary where the cavity potential becomes repulsive and the head group anions are anchored.

Table 4. Percentage of water in each region based on the O atom radial density profiles for K$^+$ and Na$^+$ (in parenthesis) RMs.

Water region	w_0			
	1	2	4	7.5
Trapped^a	14 (28)	20 (32)	20 (33)	16 (22)
Bound^b	75 (62)	56 (49)	49 (37)	39 (31)
Free	11 (10)	23 (19)	31 (30)	45 (47)

^{a} $D<0.5$ Å.
^{b} The bound and free water regions are separated at the third minimum in the density in the Na$^+$ RMs ($D{\sim}4$–5 Å).
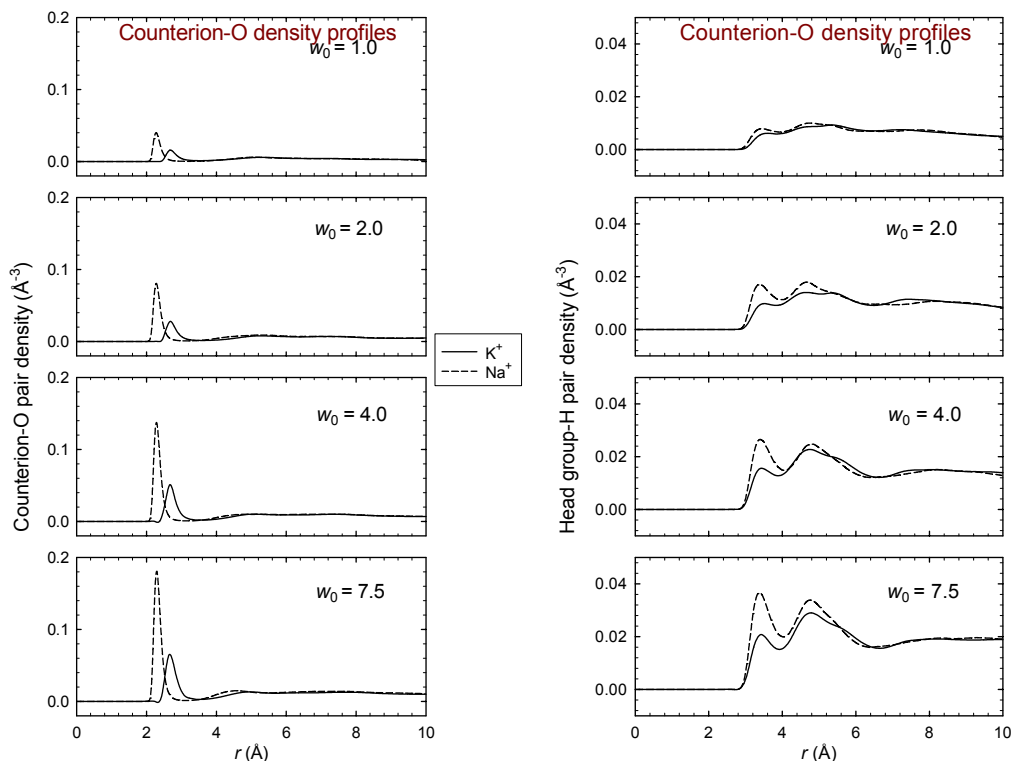
9

Figure 3. Counterion-water oxygen (left) and head group - water hydrogen (right) pair densities. The average water density (unnormalized) is plotted as a function of distance from the counterion or head group. Solid lines are for K^+ RMs, dashed lines are for Na^+ RMs.

The counterion density profiles shown in the right panel of Fig. 2 reflect the significant differences in the coordination structure of the ionic layer. The Na^+ density profiles in the interfacial region are characterized by a sharp peak near $D = 0$ Å, corresponding with highly coordinated "lattice" counterions, and a second, broader peak near $D = 1$ Å that shifts toward the interface and becomes more diffuse with increasing RM size. In contrast, the K^+ counterion distribution consists of a single broad peak centered near $D = 0$ Å that shifts away from the interface slightly (0.25 Å) with increasing RM size. At all RM sizes the density of counterions dissolved in the interior is much lower for K^+ than for Na^+. The broadening and shifting of the lattice counterion peak away from $D = 0$ Å for the K^+ counterions is probably due to its interactions with water in both the trapped and bound water layers. Because of their larger size, the K^+ ions are able to remain highly coordinated near the interface and still maintain substantial interactions with water in the bound layer. Na^+ ions, on the other hand, must move farther from the interface to coordinate water molecules in the bound layer, which results in two distinct states—one with higher ionic coordination and one with higher water coordination—as reflected by the bimodal distribution of counterions. As the surface ion density decreases, multiple ionic

10

coordination becomes less important and the lattice peak disappears in the Na^+ case. Furthermore, despite the stronger interactions of Na^+ with the head group ions, lattice formation is less favorable with the smaller counterions because of packing considerations and the Na^+ ions are therefore freer to migrate away from the interface to interact with water in the bound layer or even to dissolve in the core. The substantially larger number of Na^+ counterions in the intermediate region between $D = 1$ and 2 Å, coupled with the stronger interactions of Na^+ with water, also explain the larger disruption of water structure in the bound water region of the larger Na^+ RMs seen in the water oxygen density profiles between $D = 4$ and 6 Å of the left panel of Fig. 2.

Figure 3 depicts the pair densities for water with counterions (left) and head groups (right). The left panel data show a higher and narrower first peak, for Na^+-O than for K^+-O pair densities, indicating clearly that water oxygen coordinates much more strongly to Na^+ than to K^+ ions. This result is expected given the bulk aqueous solution structural data for the two ions.[29,35-40] What is surprising is the impact of the differences in counterion size on water-head group pair correlations. The right panel of Fig. 3 shows that there is a substantial decrease in the height of the first peak in the head group-H pair densities in K^+ relative to Na^+ RMs. Thus, even though the head group-water potential is the same in both systems, the H-head group coordination is strongly suppressed in the presence of K^+ counterions. As was already noted in connection with the density profile data shown in Fig. 2, K^+ ions tend to pack more efficiently at the interface and displace water from the head group vicinity to a larger extent than do Na^+ ions. The suppression of H-headgroup coordination is a consequence of this fact.

While water–headgroup hydrogen bonding decreases in the K^+ RMs, water–water hydrogen bonding increases, as shown in Fig. 4, which plots of the average number of hydrogen bonds per water molecule as a function of D. Two water molecules are considered hydrogen-bonded if their pair interaction energy is more negative than -16 kJ/mol.[41] The amount of hydrogen-bonding per water molecule increases nearly linearly from a small value at the interface until it reaches a plateau near the bulk value at about $D = 5$ Å. There is more hydrogen bonding at all distances with K^+ than with Na^+, consistent with the expectation that the smaller counterion will produce greater disruption of water hydrogen bonding, particularly in its first solvation shell. It is notable that there is always a substantial difference in water hydrogen bonding in the region nearest the interface and that in the larger RMs this is the region with the largest difference. While the strong Na^+–water interactions nearly eliminate water–water

hydrogen bonding in the trapped water region, the weaker K^+–water interactions permit a significant amount of hydrogen bonding even though the density of water at the interface is only about half as large. Note that there is almost no difference in water density between the Na^+ and K^+ RMs by a distance of 1 Å from the interface, where a water molecule trapped at D=0 Å is most likely to find a hydrogen bonding partner.
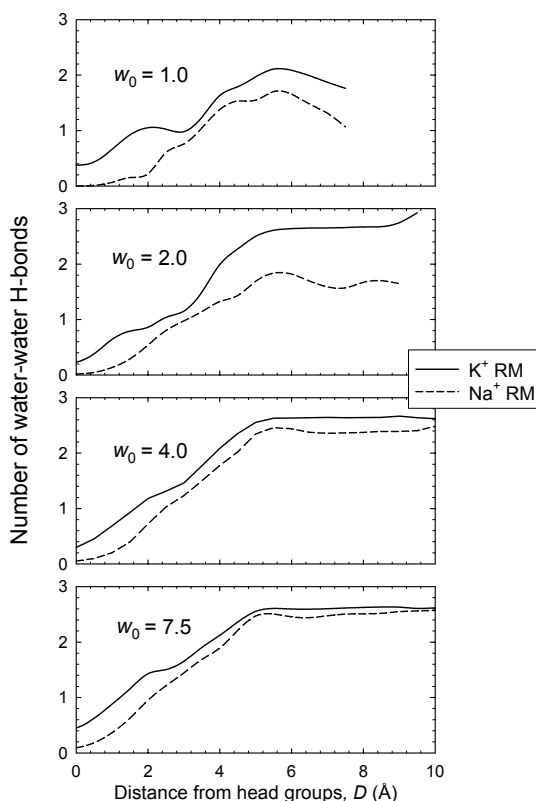

Figure 4. Average number of water-water hydrogen bonds per water molecule as a function of distance from the interface (D). The pair energy threshold used to determine hydrogen bonding is –16 kJ/mol.

The translational and rotational mobilities of water, presented in Table 5 and Fig. 5 respectively, also demonstrate that water in the K^+ RMs is less affected by the RM environment. Table 5 presents the effective water diffusion coefficients that are determined from a linear fit to the mean-squared center-of-mass displacements over the time interval between 2 and 10 ps. The diffusion coefficient for a given region of the RM is obtained by averaging over water molecules that start in that region at zero time. For RM sizes $2 \leq w_0 \leq 7.5$, the overall trends in mobility are the same for the two different counterions. Mobility within a region increases with RM size, and mobility within a given RM size increases with distance from the interface, approaching the bulk value in the most interior regions of the largest RMs.

In the case of K^+ RMs, but not for Na^+ RMs, the trend in the size dependence of water mobility is reversed for the smallest RM sizes, with somewhat higher mobilities in the trapped and bound regions observed for $w_0 = 1$ than for $w_0 = 2$. The same trend is also observed for the rotational mobility, although the data for $w_0 = 1$ is not shown in Fig. 5. The reason for this reversal appears to be that about 30% of water molecules in the trapped layer of the $w_0 = 2$ K^+ RM have two counterions in their first coordination shell, which it is quite rare in all the other systems studied. This multiple counterion coordination can be expected to decrease the mobility of the water molecules affected and to disrupt the water hydrogen bond network. Figure 4 shows that there is a decreased level of water-water hydrogen bonding at the interface of the $w_0 = 2$ K^+ RM in comparison to $w_0 = 1$, where the density of water at the interface is considerably lower. It thus appears that, at least for the K^+ counterion, there is a w_0 where the mobility of interfacial water is minimized because it is optimally incorporated into the surface ionic layer.

Water mobility by region and size is nearly always higher in the K^+ RMs than in the Na^+ RMs. The only exceptions to this trend involve translational mobility differences of less than 10% in the free water regions of the largest two RMs. Counterion size has a large effect on water mobility primarily in the trapped water region, where mobility in the K^+ RMs is increased by a factor of about 2–10 that generally decreases with RM size.   The weaker interaction between water and the larger K^+ counterions appears to be the dominant factor affecting its translational and rotational mobility.

Table 5. Effective water diffusion coefficients (10^{-9} m^2 s^{-1}) by region from mean-squared displacements for K^+ and Na^+ (in parentheses) RMs. [a]

Water Region[b]	w_0			
	1	2	4	7.5
Trapped	0.40 (0.05)	0.20 (0.04)	0.55 (0.28)	0.90 (0.36)
Bound	1.16 (1.05)	1.10 (1.01)	1.15 (1.16)	1.39 (1.25)
Free I	1.14 (0.84)	1.50 (0.96)	1.65 (1.76)	1.91 (1.86)
Free II	–	–	1.96 (2.23)	2.26 (2.23)
Free III	–	–	–	2.46 (2.51)

[a] Bulk diffusion coefficient of SPC/E water is 2.50×10^{-9} m^2 s^{-1}.
[b] Classification is the same as in Table 4 except that the free water region is divided into 3 Å bins.
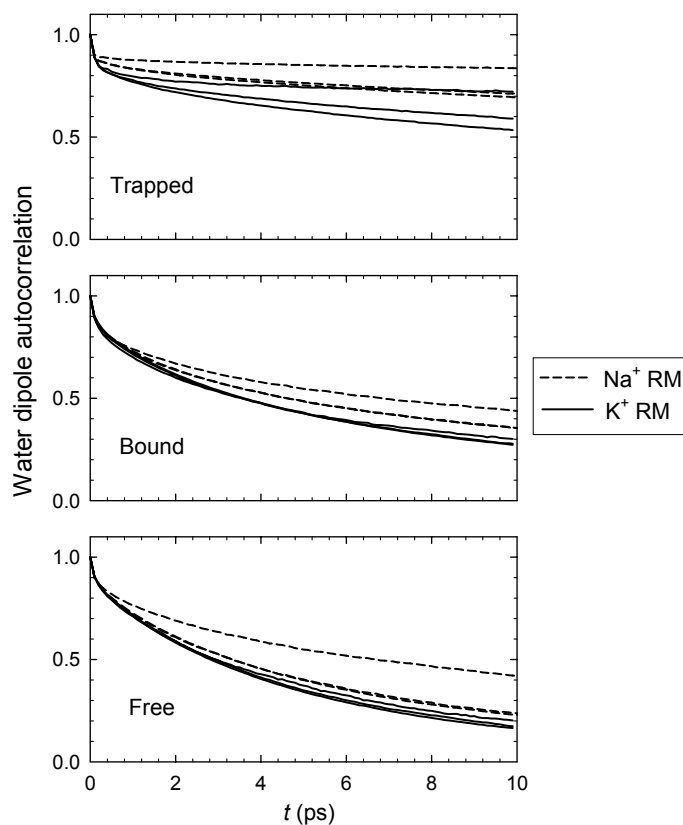
Figure 5. Water dipole-dipole autocorrelation functions by region within the micelle for $w_0 = 2$, 4, and 7.5. The classification of each water molecule at the time origin determines the average to which it contributes. For both counterions within each region the rate of relaxation always increases with w_0.

IV. Conclusions

We have presented a study of the effects of counterion size on the properties of the interior region of model RMs in the water content range $1 \leq w_0 \leq 7.5$. Our model systems were designed to represent water-in-oil microemulsions formed by KAOT and NaAOT surfactants. There are four primary molecular interactions in the model—counterion–head group anion, counterion–water, water–head group anion, and water–water—and increasing the counterion size directly decreases the strength of only the first two of these interactions. This decrease results in the expected increases in water mobility and the bulk-like propreties of water near the interface, as reflected in water-water hydrogen bonding.

Less anticipated is the effect of counterion size on the structure of the ionic layer at the interface. The larger counterions display greater coordination with the anionic head groups, are more effective at excluding water from the interfacial layer, and are much less likely to dissolve into the RM core. More favorable packing of the larger K^+ counterions at the interface is

14

responsible for these trends. In addition, the counterion density as a function of distance from the interface displays less sensitivity to increasing RM size and does not split into two peaks as observed in the Na^+ RMs. The latter observation appears to be the result of the larger counterion's ability to simultaneously maintain multivalent interactions with the ionic layer and the intermediate layer of bound water.

Despite differences in the ionic layer, the basic layered structure of water at the RM interface is preserved, and the primary difference in the water density profiles observed in the K^+ RMs is the decreased size of the peak correpsonding to water trapped in the ionic layer. Other than the height of the trapped water peak, the structure of the water profiles appears to be minimally affected in the two smaller RMs. In the two larger RMs, the density profiles in the region 4–6 Å from the interface appear to be more structured in the Na^+ RMs as a result of the greater disruption of the water structure by the Na^+–water interaction and because of the greater migration of Na^+ counterions away from the interface.

The combination of greater exclusion of water from the interface and its weaker attraction to K^+ result in smaller disruption in water structure and in higher water mobility in K^+-based relative to Na^+ based RMs. The number of water-water hydrogen bonds in the interfacial layers is greater and approaches a bulk-like value nearer the interface in K^+ RMs than in Na^+ RMs at of a given w_0. The decrease in trapped water also reduces the amount of water-head group anion hydrogen bonding, which is interesting because the strength of this interaction is not directly affected by the nature of the counterion. We also found that the water orientational relaxation rates and translational diffusion coefficients are larger in the K^+ RMs than in Na^+ RMs, with the most significant differences occurring in the trapped water layer. The differences generally decrease with increasing RM size and, for a given w_0, with increasing distance from the interface.

The simulated effects on water structure and mobility may be compared with two studies that examined the effect of substituting K^+ for Na^+ in water/AOT/isooctane RMs. Using infrared spectroscopy of the water OH stretch region, Temsamani et al. [25] found that water-headgroup hydrogen bonding increased with water content, but that for a given w_0 the size of the alkali counterion had only a small effect on the extent of water-head group hydrogen bonding. As shown in the right panel of Fig. 3, the simulations find that water-headgroup hydrogen bonding increases with RM size, but that the hydrogen bonding is decreased in the K^+ RMs by an amount that is larger (10–40%) than is observed in the experiments. Many factors could give rise to this

discrepancy, not the least of which are the unknown effects that such a strongly ionic environment might have on the water environment. A proper comparison between the MD results and the experiments would require us to simulate the water IR spectrum directly, which would be a worthwhile subject for future investigations. The atomic structure of the SO_3^- headgroup, approximated by a single united atom site in the current model, may also affect the structure of the interface and the strength of water-headgroup interactions, and a model removing this approximation is currently under development.

The studies by Pant et al. [24] of the effect of counterion substitution on solvation dynamics inside RMs are more in accord with the current results. They found that water mobility, as measured by the timescales for solvent relaxation, increases both with increasing water content and counterion size. They also observed that solvent relaxation was much faster in highly concentrated ionic solutions designed to mimic the average ion concentrations found in the interior of low water content RMs. This is most dramatically reflected in the absence of long-time (>10 ps) component in the solvent relaxation that is a small but characteristic feature of the water response in complex environments.[24,42] The absence of these long-time components in concentrated ionic solutions and their presence in RMs is explained by the layered structure of the RM interior observed in our simulations. The concentration of ions in the interfacial layer results in a much higher local concentration than can be obtained in bulk solution, and results in a substantial slowdown of both water and counterion motion in this layer. The trapped counterion and water layer remains a constant feature of RMs even as the water content and counterion size are increased, and results in a significant long time component in the solvent relaxation in all the RM systems studied.[13]

In conclusion, these results, several of which were difficult to anticipate in advance, demonstrate the utility of our simple molecular model of the RM interior for systematically investigating the properties of these complex nanoscale assemblies.

Acknowledgments

References and Notes

(1)   de Gennes, P. G.; Taupin, C. *J. Phys. Chem.* **1982**, *86*, 2294.

(2)   Langevin, D. *Acc. Chem. Res.* **1988**, *21*, 255.

(3)   Chevalier, Y.; Zemb, T. *Rep. Prog. Phys.* **1990**, *53*, 279.

(4)   *Micelles, Membranes, Microemulsions, and Monolayers*; Gelbart, W. M.; Ben-Shaul, A.; Roux, D., Eds.; Springer: Berlin, 1994.

(5)   Gelbart, W. M.; Ben-Shaul, A. *J. Phys. Chem.* **1996**, *100*, 13169.

(6)   Moulik, S. P.; Paul, B. K. *Adv. Colloid Interface Sci.* **1998**, *78*, 99.

(7)   Luisi, P. L.; Giomini, M.; Pileni, M. P.; Robinson, B. H. *Biochim. Biophys. Acta* **1988**, *947*, 209.

(8)   Luisi, P. L.; Straub, B. E. *Reverse Micelles: Biological and Technological Relevance of Amphiphilic Structures in Apolar Media*; Plenum: New York, 1984.

(9)   De, T.; Maitra, A. *Adv. Colloid Interface Sci.* **1995**, *59*, 95.

(10)   Pileni, M. P. *J. Phys. Chem.* **1993**, *97*, 6961.

(11)   Pileni, M. P. *Langmuir* **1997**, *13*, 3266.

(12)   Faeder, J.; Ladanyi, B. M. *J. Phys. Chem. B* **2000**, *104*, 1033.

(13)   Faeder, J.; Ladanyi, B. M. *J. Phys. Chem. B* **2001**, *105*, 11148.

(14)   Eicke, H. F.; Rehak, J.; Phys.-Chem. Inst, U. B. B. S. *Helv. Chim. Acta* **1976**, *59*, 2883.

(15)   Eastoe, J.; Robinson, B. H.; Heenan, R. K. *Langmuir* **1993**, *9*, 2820.

(16)   Eastoe, J.; Towey, T. F.; Robinson, B. H.; Williams, J.; Heenan, R. K. *Journal of Physical Chemistry* **1993**, *97*, 1459.

(17)   Eastoe, J.; Chatfield, S.; Heenan, R. *Langmuir* **1994**, *10*, 1650.

(18)   Eastoe, J.; Steytler, D. C.; Robinson, B. H.; Heenan, R. K.; Norht, A. N.; Dore, J. C. *Journal of the Chemical Society-Faraday Transactions* **1994**, *90*, 2497.

(19)   Giordano, R.; Migliardo, P.; Wanderlingh, U.; Bardez, E.; Vasi, C. *Journal of Molecular Structure* **1993**, *296*, 265.

(20)   Camardo, M.; Dangelo, M.; Mannaioli, S.; Onori, G.; Santucci, A. *Colloids and Surfaces a-Physicochemical and Engineering Aspects* **1996**, *119*, 183.

(21)   Fioretto, D.; Freda, M.; Onori, G.; Santucci, A. *Journal of Physical Chemistry B* **1999**, *103*, 8216.

(22)   Fioretto, D.; Freda, M.; Mannaioli, S.; Onori, G.; Santucci, A. *Journal of Physical Chemistry B* **1999**, *103*, 2631.

(23)   Riter, R. E.; Undiks, E. P.; Levinger, N. E. *J. Am. Chem. Soc.* **1998**, *120*, 6062.

(24)   Pant, D.; Riter, R. E.; Levinger, N. E. *J. Chem. Phys.* **1998**, *109*, 9995.

(25)   Temsamani, M. B.; Maeck, M.; El Hassani, I.; Hurwitz, H. D. *Journal of Physical Chemistry B* **1998**, *102*, 3335.

(26)   Lee, C. Y.; McCammon, J. A.; Rossky, P. J. *J. Chem. Phys.* **1984**, *80*, 4448.

(27)   Borin, I. A.; Ladanyi, B. M. manuscript in preparation, 2002.

(28)   Berendsen, H. J. C.; Grigera, J. R.; Straatsma, T. P. *J. Phys. Chem.* **1987**, *91*, 6269.

(29)   Dang, L. X. *Journal of the American Chemical Society* **1995**, *117*, 6954.

(30)   Allen, M. P.; Tildesley, D. J. *Computer Simulation of Liquids*; Clarendon: Oxford, U.K., 1987.

(31)   Berendsen, H. J. C.; Postma, J. P. M.; van Gunsteren, W. F.; DiNola, A.; Haak, J. R. *J. Chem. Phys.* **1984**, *81*, 3684.

(32)   Griffiths, J. A.; Heyes, D. M. *Langmuir* **1996**, *12*, 2418.

(33)   Allen, R.; Bandyopadhyay, S.; Klein, M. L. *Langmuir* **2000**, *16*, 10547.

(34)   Salaniwal, S.; Cui, S. T.; Cochran, H. D.; Cummings, P. T. *Langmuir* **2001**, *17*, 1773.

(35)   Enderby, J. E. *Annual Review of Physical Chemistry* **1983**, *34*, 155.

(36)   Impey, R. W.; Madden, P. A.; McDonald, I. R. *Journal of Physical Chemistry* **1983**, *87*, 5071.

(37)   Bounds, D. G. *Molecular Physics* **1985**, *54*, 1335.

(38)   Enderby, J. E. *Pure and Applied Chemistry* **1985**, *57*, 1025.

(39)   Enderby, J. E.; Cummings, S.; Herdman, G. J.; Neilson, G. W.; Salmon, P. S.; Skipper, N. *Journal of Physical Chemistry* **1987**, *91*, 5851.

(40)   Neilson, G. W.; Enderby, J. E. *Advances in Inorganic Chemistry* **1989**, *34*, 195.

(41)   Linse, P. *J. Chem. Phys.* **1989**, *90*, 4992.

(42)   Bhattacharyya, K.; Bagchi, B. *J. Phys. Chem. A* **2000**, *104*, 10603.